RSC Advances

PAPER

View Article Online
View Journal | View Issue

Cite this: *RSC Adv.*, 2021, **11**, 21433

Antioxidant and UV-radiation absorption activity of aaptamine derivatives – potential application for natural organic sunscreens†

Thi Le Anh Nguyen, *[ab] Thi Hoai Nam Doan,[c] Dinh Hieu Truong,[ab] Nguyen Thi Ai Nhung,[d] Duong Tuan Quang,[e] Dorra Khiri,[f] Sonia Taamalli,[f] Florent Louis,[f] Abderrahman El Bakali[f] and Duy Quang Dao *[a]

Antioxidant and UV absorption activities of three aaptamine derivatives including piperidine[3,2-*b*] demethyl(oxy)aaptamine (**C1**), 9-amino-2-ethoxy-8-methoxy-3*H*-benzo[de][1,6]naphthyridine-3-one (**C2**), and 2-(*sec*-butyl)-7,8-dimethoxybenzo[de]imidazo[4,5,1-*ij*][1,6]-naphthyridin-10(9*H*)-one (**C3**) were theoretically studied by density functional theory (DFT). Direct antioxidant activities of **C1–C3** were firstly evaluated *via* their intrinsic thermochemical properties and the radical scavenging activity of the potential antioxidants with the HOO˙/HO˙ radicals *via* four mechanisms, including: hydrogen atom transfer (HAT), single electron transfer (SET), proton loss (PL) and radical adduct formation (RAF). Kinetic calculation reveals that HOO˙ scavenging in water occurs *via* HAT mechanism with **C1** (k_{app}, 7.13 × 10^6 M^{-1} s^{-1}) while RAF is more dominant with **C2** (k_{app}, 1.40 × 10^5 M^{-1} s^{-1}) and **C3** (k_{app}, 2.90 × 10^5 M^{-1} s^{-1}). Antioxidant activity of aaptamine derivatives can be classified as **C1** > **C3** > **C2**. Indirect antioxidant properties based on Cu(I) and Cu(II) ions chelating activity were also investigated in aqueous phase. All three studied compounds show spontaneous and favorable Cu(I) ion chelating activity with ΔG^0 being −15.4, −13.7, and −15.7 kcal mol^{-1}, whereas ΔG^0 for Cu(II) chelation are −10.4, −10.8, and −2.2 kcal mol^{-1} for **C1**, **C2** and **C3**, respectively. In addition, all compounds show UVA and UVB absorption; in which the excitations are determined mostly as π−π* transition. Overall, the results suggest the potential applications of the aaptamines in pharmaceutics and cosmetics, *i.e.* as a sunscreen and antioxidant ingredient.

Received 28th May 2021
Accepted 11th June 2021

DOI: 10.1039/d1ra04146k

rsc.li/rsc-advances

1. Introduction

Aaptamines are commonly known natural products, which have been extracted from *Aaptos aaptos* species in the marine milieu of the Pacific ocean, *i.e.* Malaysia,[1] Vietnam,[2] and Indonesia.[3] The first aaptamine structures, extracted from a Japanese sponge and characterized by Nakamura *et al.*,[4] are identified as alkaloid-based compounds containing the 1*H*-benzo[de]-1,6-naphthyridine skeleton. There is a large amount of research which reported different biological activities of aaptamines such as antifungal,[5,6] antiviral,[7] antimicrobial,[8] and anticancer.[1,9–13] In particular, antioxidant activity of aaptamines was early predicted and studied. Indeed, aaptamines and isoaaptamine, amongst other marine sponges, were reported for strong antioxidant activity against the DPPH radical.[14] In a perspective view, besides the natural and well-disposed origin, the antioxidant properties and other biological activities of the aaptamines can be of human-health-benefit because they help protect the human body from free radicals, fight aging, boost the immune system, and prevent diseases. In the modern concept of antioxidants, it is noteworthy that the antioxidant properties of a compound are based not only on the free radical scavenging processes but also on the repairing activity for biomolecules, such as DNA, lipid or proteins, and on the chelating ability with oxidative transition metal ions, particularly Cu[15–19] and Fe ions.[20–22] The latter plays an important role in preventing the indirect formation of reactive hydroxyl radical (*i.e.* HO˙) caused by the Fenton-like reactions between Fe(II) and Cu(I) with hydrogen peroxide (*i.e.* H_2O_2).

On the other hand, oxidative stress (OS) resulting from long-time ultraviolet radiation (UVR) exposure is identified as one of the main causes for skin aging, DNA skin damage and melanogenesis.[23] At the early stage of the sunscreen research started

[a]*Institute of Research and Development, Duy Tan University, Da Nang, 550000, Vietnam. E-mail: nguyenthileanh@duytan.edu.vn; daoduyquang@duytan.edu.vn*
[b]*Faculty of Natural Sciences, Duy Tan University, Da Nang, 550000, Vietnam*
[c]*Department of Chemistry, Danang University of Science and Technology, The University of Danang, Da Nang, 550000, Vietnam*
[d]*Department of Chemistry, University of Sciences, Hue University, Hue, 530000, Vietnam*
[e]*Department of Chemistry, University of Education, Hue University, Hue, 530000, Vietnam*
[f]*Université de Lille, CNRS, UMR 8522, PC2A – PhysicoChimie des Processus de Combustion et de l'Atmosphère, 59000 Lille, France*

† Electronic supplementary information (ESI) available. See DOI: 10.1039/d1ra04146k

by the 1940s, most of the products targeted minimizing the effect of UVB (280–315 nm) radiation because the direct UVB absorption by DNA generates UV-signature mutations leading to DNA lesions and carcinogenic effect.[24] Scientists later discovered that the UVA (315–400 nm) can deeply penetrate into the skin, producing reactive oxygen species (ROS) and reactive nitrogen species (RNS) in human skin that cause DNA as well as other biological molecules to be damaged and so is not less harmful than the UVB to human skin.[25,26] One of the common mechanism, for example, is the ROS-mediated cell damage by peroxidation of fatty acids within the phospholipid structure of the membrane. Recently, a broad-spectrum UV filter that covers both UVA and UVB regions is one of the first and foremost criteria for considering an organic sunscreen candidate.[27]

Moreover, the photo-protective properties of natural products have been earlier reported for natural antioxidants including polyphenols,[28] stilbenes,[29] hydroxycinamate derivatives.[30,31] A large number of studies have shown positive effect of antioxidant in the skin, for both treatment and prevention of inflammation, oxidation, sebaceous glands or melanogenesis.[32] Multiple mechanisms of skin photo-protective have been documented.[26] In addition, the synthesis of *p*-hydroxycinnamic diacids such as of ferulic, sinapic, *p*-coumaric and caffeic diacid results in molecules which show potent antioxidant and UV filter.[33] Recently, we reported the antioxidant and photo-protective properties of different natural compounds in which the cycloechinulin and wasabidienone extracted from marine fungus showed the most potential antioxidant and photo-protective properties.[34]

To the best of our knowledge, although some experimental studies have been performed on the antioxidant properties of aaptamines derivatives, there have not been any computational studies that consider both radical scavenging and photo-protective properties of the aaptamine derivatives. Thus, in this study the antioxidant activities and the UV filter properties of three aaptamine derivatives[4] including piperidine[3,2-*b*] demethyl(oxy)aaptamine (**C1**), 9-amino-2-ethoxy-8-methoxy-3*H*-benzo[de][1,6]naphthyridine-3-one (**C2**), and 2-(*sec*-butyl)-7,8-dimethoxybenzo[de]imidazo[4,5,1-*ij*][1,6]-naphthyridin-10(9*H*)-one (**C3**) (Fig. 1) were elucidated using density functional theory (DFT). Multi-level thermodynamic and mechanistic approaches were applied to provide better insight into direct antioxidant properties based on the free radical scavenging reactions. Thermodynamic parameters of reaction characteristic of the antioxidant activity of three aaptamines **C1–C3** *via* four common mechanisms: hydrogen transfer (HT), single electron transfer (SET), proton loss (PL), and radical adduct formation (RAF) were focused. Different intrinsic thermochemical parameters including bond dissociation enthalpy (BDE), adiabatic ionization potential (IP) and proton affinity (PA) were calculated in the gas phase (*vacuo*) and water. The reaction enthalpies ($\Delta_r H^0$) and standard Gibbs free energies ($\Delta_r G^0$) of four reactions between the studied compounds and HOO$^\bullet$/HO$^\bullet$ radicals were examined and the kinetic calculations were investigated using transition state theory (TST). Remarkably, indirect antioxidant properties based on the Cu(II) ion chelating activity of studied compounds in aqueous phase were also predicted. Finally, the time-dependent density functional theory (TD-DFT) was performed to study the UV absorption activities of the aaptamines. Hopefully, the obtained results contribute to a better understanding of the antioxidant and UVR absorption properties of marine product which allows further practical applications.

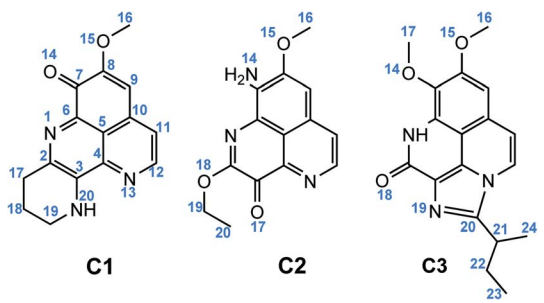

Fig. 1 Chemical structure of **C1–C3**.

2. Computational details

Gaussian 16 revision A.03 package was used to optimize the geometrical and electronic structures of the studied compounds.[35] All calculations were performed at the M05-2X/6-311++G(d,p) level of theory.[36] The M05-2X is previously reported to have a good benefit for the TS location and kinetics calculation.[37,38]

The four main working mechanisms, including formal hydrogen transfer (FHT), single electron transfer (SET), proton loss (PL) and radical adduct formation (RAF) have been investigated. In the first approach, the intrinsic thermochemical parameters characterizing for three mechanisms FHT, SET, and PL were calculated according to the following reaction equations:

Formal hydrogen transfer (FHT):

$$\text{A–H} \rightarrow \text{A}^\bullet + \text{H}^\bullet \text{ (BDE)}; \quad \text{(R1)}$$

Single electron transfer (SET):

$$\text{A–H} \rightarrow \text{AH}^{+\bullet} + \text{e}^- \text{ (IP)}; \quad \text{(R2)}$$

Proton transfer (PT):

$$\text{A–H} \rightarrow \text{A}^- + \text{H}^+ \text{ (PA)}; \quad \text{(R3)}$$

Based on the equations (R1)–(R3), intrinsic thermodynamic parameters such as bond dissociation enthalpies (BDE), adiabatic ionization potential (IP), and proton affinities (PA) were calculated in the gas phase and in water as follows:

$$\text{BDE (A–H)} = H(\text{A}^\bullet) + H(\text{H}^\bullet) - H(\text{A–H}); \quad (1)$$

$$\text{IP (A–H)} = H(\text{AH}^{\bullet+}) + H(\text{e}^-) - H(\text{A–H}); \quad (2)$$

$$\text{PA (A–H)} = H(\text{A}^-) + H(\text{H}^+) - H(\text{A–H}); \quad (3)$$

where H accounts for the total energy of the studied specie at 298.15 K and 1 atm. The experimental energy value of the proton (H^+) and the electron (e^-) in gas phase was 1.4811 and 0.7519 kcal mol^{-1}, respectively.[39] In water, the energy values of

proton $H(H^+)$ and of electron $H(e^-)$ were −235.3 and −23.9 kcal mol^{-1}, respectively; calculation method was previously reported.[40]

In order to evaluate the influence of chemical nature of free radicals on the antioxidant potential of the studied compounds *vs.* representative radicals such as HOO$^\bullet$, the standard Gibbs free energies of the reaction ($\Delta_r G^0$) were calculated for HAT, PL, RAF and SET mechanisms according to the (R4)–(R7) reactions ((4)–(7)). The HO$^\bullet$ radical scavenging reactions were similarly obtained.

$$\text{FHT: A–H + HOO}^\bullet \rightarrow \text{A}^\bullet + \text{HOOH}; \quad \text{(R4)}$$

$$\text{PL: A–H + HOO}^\bullet \rightarrow \text{A}^- + \text{HOOH}^{\bullet+}; \quad \text{(R5)}$$

$$\text{RAF: A–H + HOO}^\bullet \rightarrow \text{AH–OOH}^\bullet; \quad \text{(R6)}$$

$$\text{SET: A–H + HOO}^\bullet \rightarrow \text{AH}^{\bullet+} + \text{HOO}^-; \quad \text{(R7)}$$

Standard Gibbs free energies ($\Delta_r G^0$) of the reactions were calculated at 298.15 K as follows:

$$\Delta_r G^0\,(\text{HAT}) = [G(\text{A}^\bullet) + G(\text{HOOH})] - [G(\text{A–H}) + G(\text{HOO}^\bullet)]; \quad (4)$$

$$\Delta_r G^0\,(\text{PL}) = [G(\text{A}^-) + G(\text{HOOH}^{\bullet+})] - [G(\text{A–H}) + G(\text{HOO}^\bullet)]; \quad (5)$$

$$\Delta_r G^0\,(\text{RAF}) = G(\text{AH–OOH}^\bullet) - G(\text{A–H}) - G(\text{HOO}^\bullet); \quad (6)$$

$$\Delta_r G^0\,(\text{SET}) = [G(\text{AH}^{\bullet+}) + G(\text{HOO}^-)] - [G(\text{HOO}^\bullet) + G(\text{A–H})]; \quad (7)$$

The kinetics of FHT and RAF reactions in the gas phase and in water studied in this work were based on quantum mechanics-based test for overall free radical scavenging activity (QM-ORSA) protocol[37] using the Eyringpy code.[41] Details of this calculation can be found in our previous work.[34] In brief, reaction rate, $k(T)$, can be calculated using conventional transition state theory (TST) approach.

$$k(T) = \sigma\kappa\frac{k_B T}{\hbar}e^{\frac{-\Delta G^\ddagger}{RT}} \quad (8)$$

where $\Delta G^\ddagger$ is the Gibbs free energy of activation; T is the temperature in Kelvin; k_B is the Boltzmann constant and $\hbar$ is the Planck constant; σ is the reaction symmetry number (or the reaction path degeneracy), κ is the transmission coefficient attributing for the quantum tunneling effects by employing Eckart barrier. The solvent cage effect was included according to the correction proposed by Okuno,[42] taking into account the free volume theory.[43]

For SET reaction, the Marcus theory[44] was applied for the estimation of the electron transfer rate. The energy barrier was obtained as (9).

$$\Delta G^\ddagger_{SET} = \frac{\lambda}{4}\left(1 + \frac{\Delta G^0_{SET}}{\lambda}\right)^2; \quad (9)$$

where ΔG^0_{SET} is the free energy of reaction; λ is the nuclear reorganization energy which can be calculated by the difference of ΔE_{SET} and ΔG^0_{SET}, with ΔE_{SET} is the vertical energy between reactants and products of the reaction *via* SET mechanism.

In solvent, diffusion rate k_D may be important and greatly contributes to the apparent rate constant k_{app}. Therefore, the Collins–Kimball theory[45] was employed (10).

$$k_{app} = k_D k/(k_D + k); \quad (10)$$

where k is the thermal rate constant and k_D is the diffusion rate constant calculated following Smoluchowski[46] (11).

$$k_D = 4\pi R_{AB} D_{AB} N_A; \quad (11)$$

where the R_{AB} is the reactant distance, D_{AB} is the mutual diffusion coefficient of the antioxidant A and radical B (HOO$^\bullet$) and N_A is the Avogadro number; D_{AB} is estimated from D_A and D_B as proposed by Truhlar[47] in which D_A and D_B are computed using the Stockes–Einstein approach[48,49] (12)

$$D_{AB} = k_B T/(6\pi\eta r); \quad (12)$$

in which η is the viscosity of water (8.91×10^{-4} P s) and r is the radius of the solute.

The pK_a calculation of three amines was performed following the thermodynamic cycle previously reported.[50,51] pK_a of the **C1–C3** were determined as (13)

$$pK_a = \Delta G^0_{deprot,aq}/RT\ln(10); \quad (13)$$

where the $\Delta G^0_{deprot,aq}$ is the solution-phase standard free energy of deprotonation.

Cu(I) and Cu(II) ions chelating processes of three antioxidant compounds, now denoted as L, occur *via* the following reactions:

$$\text{L} + [\text{Cu}\cdot 4\text{H}_2\text{O}]^+ = [\text{CuL}\cdot 2\text{H}_2\text{O}]^+ + 2\text{H}_2\text{O}; \quad \text{(R8)}$$

$$\text{L} + [\text{Cu}\cdot 4\text{H}_2\text{O}]^{2+} = [\text{CuL}\cdot 2\text{H}_2\text{O}]^{2+} + 2\text{H}_2\text{O}; \quad \text{(R9)}$$

The Gibbs free energies ($\Delta_r G^0$) of the complex formation were then calculated by (14) and (15) as follows:

$$\Delta_r G^0[\text{Cu(I)}] = G([\text{CuL}\cdot 2\text{H}_2\text{O}]^+) + 2G(\text{H}_2\text{O}) - G(\text{L}) - G([\text{Cu}\cdot 4\text{H}_2\text{O}]^+); \quad (14)$$

$$\Delta_r G^0[\text{Cu(II)}] = G([\text{CuL}\cdot 2\text{H}_2\text{O}]^{2+}) + 2G(\text{H}_2\text{O}) - G(\text{L}) - G([\text{Cu}\cdot 4\text{H}_2\text{O}]^{2+}); \quad (15)$$

The standard enthalpies of reaction (ΔH^0) were similarly calculated for the complexation reaction (R8) and (R9).

The vertical excitation of **C1–C3** in methanol was calculated using TD-DFT approach. A small benchmark of functionals with different exchange correlation XC part, *i.e.* B3LYP, B98, M06, PBE0, CAMB3LYP, and M05-2X were employed with the same basis set as in the previous part. These functionals are chosen following the recommendation by Jacquemine *et al.* for low Mean Signed Error (MSE) and Mean Absolute Error (MAE) for singlet excited states.[52] Solvent effects were implicitly studied using the Polarization Continuum Model (IEF-PCM).[53]

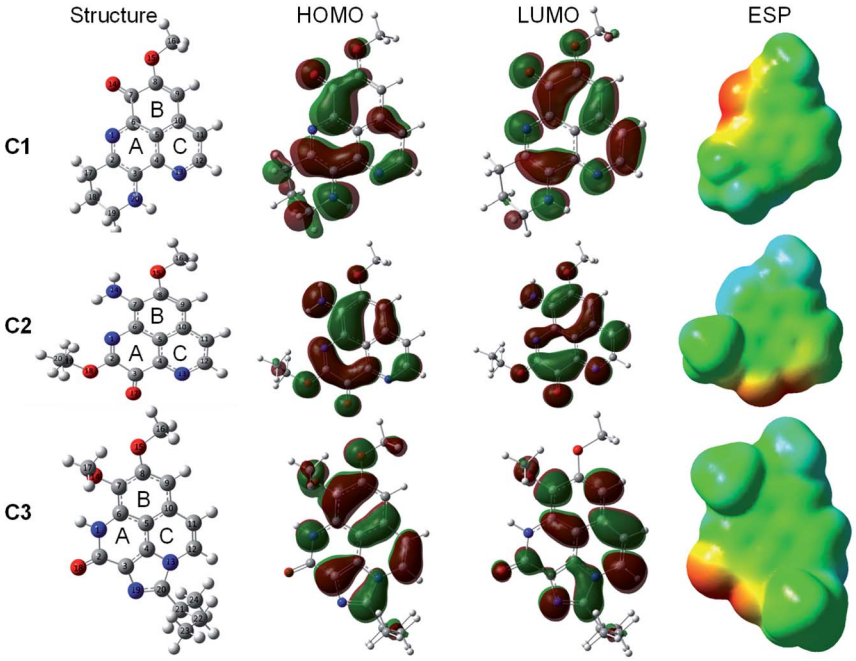

Fig. 2 Optimized geometry, HOMO, LUMO, and ESP maps of **C1–C3** calculated in the gas phase at the M05-2X/6-311++G(d,p) level of theory (isovalue = 0.02).

3. Results and discussion

3.1. Structure and electronic properties

The optimized geometry and electronic structure of the three studied aaptamine compounds calculated by DFT method at the M05-2X/6-311++G(d,p) level of theory in the gas phase are presented in the Fig. 2. Cartesian coordinates and thermochemical properties of three aaptamines derivatives are resumed in Table S1 of ESI file.†

Compounds **C1–C3** share the benzo[de][1,6]naphthyridine skeleton and similarly have $-OCH_3$ group attached to C8 position. At C7 position, the substituent groups such as ketone (=O), amine ($-NH_2$) and methoxy ($-OCH_3$) are attached to the B ring, in **C1**, **C2** and **C3**, respectively. The main difference in the chemical nature of three compounds is the substituent groups found at the A ring, for **C1** a N-containing six-membered cycle, for **C2** the =O and $-OC_2H_5$ groups, and for **C3** a N-containing five-membered cycle with 2-butyl derivative that shared both A and C ring. Moreover, the electronic distribution on the frontier molecular orbitals such as the highest occupied molecular orbital (HOMO) and the lowest unoccupied molecular orbital (LUMO) shows that all the rings play a key role in electron-donating (HOMO distribution) and electron-accepting (LUMO distribution) reactions with free radicals. For all molecules, the electrostatic potential (ESP) maps display a negative region on the C=O groups and the nearby carbons.

3.2. Evaluation of antioxidant potential *via* intrinsic thermochemical parameters

Table 1 presents the intrinsic thermochemical parameters such as BDE, IP and PA which are examined *via* the FHT (R1), SET (R2) and PL (R3) mechanisms, respectively.

Table 1 BDE, PA and adiabatic IP values (in kcal mol^{-1}) of the **C1–C3** calculated in the gas phase at the M05-2X/6-311++G(d,p) level of theory. Corresponding values in water are given in parentheses

C1				**C2**				**C3**			
Pos.	BDE	PA	IP	Pos.	BDE	PA	IP	Pos.	BDE	PA	IP
C9	111.8	371.6	168.6(110.0)	C9	113.9	366.7	168.3(109.2)	C9	113.7	368.9	169.3(114.0)
C11	114.3	374.4		C11	113.5	376.3		C11	114.9	371.3	
C12	106.2	383.6		C12	107.3	387.6		C12	114.4	360.6	
C16	97.1	367.1		C16	97.6	384.4		C16	96.5	384.2	
C17	85.5(85.6)	366.4		C19	94.7	377.8		C17	97.3	389.3	
C18	98.9	390.7		C20	100.8			C21	84.6(84.9)	366.3	
C19	85.7(79.7)	361.7		N14	92.4(91.6)	343.5(59.6)		C22	95.6	396.0	
C20	93.2	342.5(60.2)						C23	99.8	360.7	
								C24	99.0	390.4	
								N1	101.8	347.2(59.7)	

The most favorable H donating positions for **C1** and **C3** are found at C–H bonds. For example, **C1** exhibits the lowest BDE at C17 and C19 positions, being 85.5 and 85.7 kcal mol^{-1}, respectively, whereas **C3** has the lowest BDE value at C21 position, *i.e.* 84.6 kcal mol^{-1}. For **C2**, the easiest breaking-bond characterized by the lowest BDE value is located at N14 position (92.4 kcal mol^{-1}). It is noteworthy that BDE values of **C1** and **C3** are much lower than that of the standard antioxidant Trolox in the gas phase (*i.e.* 91.1 kcal mol^{-1}).[54] Consequently, the antioxidant potential of these aaptamines *via* FHT process can be classified in the following order: **C2** < Trolox < **C1** < **C3**. We observed a very slight change of BDE values in water for all compounds **C1–C3**. This result is as expected, taken into account the neutral nature of the H atom species that is transferred. The only exception is obtained for **C1** at C19 position, with a BDE value lowering from 85.7 kcal mol^{-1} in gas phase to 79.7 kcal mol^{-1} in water.

The proton donating reaction from the aaptamines to free radical is characterized by the proton affinity (PA, (3)); the lower the PA value, the better the antioxidant potential. As can be seen in Table 1, the lowest PA values are found to be 342.5, 343.5 and 347.2 kcal mol^{-1} for **C1** (at C20 position), **C2** (at N14 position) and **C3** (at N1 position), respectively. These PA values are quite similar to that of cembrene in the gas phase (*i.e.* 343.2 kcal mol^{-1}). The proton donating ability of the three compounds in reaction with free radical according to the PL process is in the increasing order: **C3** < cembrene ≈ **C2** < **C1**. It is noteworthy that the PL is much preferred in water, for which the PA values are significantly reduced about 60 kcal mol^{-1}. The result is totally in agreement with the nature of the charge specie that is given and with previously reported results.[55]

Ionization potential (IP), characteristic for SET mechanism, is the minimum energy required to transfer an electron from the studied compound to free radical to form cationic species at ground state. The lower the IP value, the easier the electron transferring ability, thus, the antioxidant activity *via* SET mechanism will be higher. According to the results presented in Table 1, the adiabatic IP of **C1–C3** varied from 168 to 169 kcal mol^{-1}, which is slightly higher than that of Trolox (*i.e.* 164.6 kcal mol^{-1}) and lower than the one of cembrene (*i.e.* 171.9 kcal mol^{-1}).[54] The antioxidant activities of the studied aaptamines following the SET mechanism increases in the order: Trolox < **C2** < **C1** < **C3** < cembrene. Similar to the proton transfer, the electron transfer is also favorable in water, with IP values reducing from 168–169 kcal mol^{-1} in gas phase to 109–114 kcal mol^{-1} in water, while remaining in the same order **C2** < **C1** < **C3**.

Overall, three aaptamines **C1–C3** are potential antioxidants. In the gas phase, the FHT mechanism can be responsible for the antioxidant properties of the molecules while in water the PL mechanism is particularly favorable.

3.3. HOO˙ and HO˙ free radical scavenging

The antioxidant potential of the studied aaptamines is investigated through the interactions with two representative free radicals, HOO˙ and OH˙, *via* four distinguished processes:

Table 2 Gibbs free energy ($\Delta_r G^0$, kcal mol^{-1}) at 298.15 K of the HAT, PL, and RAF reaction of **C1–C3** towards HOO˙ radical in the gas phase. Corresponding values calculated in water are given in parentheses for the most spontaneous reactions only. All calculations are performed at the M05-2X/6-311++G(d,p) level of theory

HAT				PL				RAF			
Pos.	**C1**	**C2**	**C3**	Pos.	**C1**	**C2**	**C3**	Pos.	**C1**	**C2**	**C3**
C9	27.3	29.5	29.2	C9	219.8	214.9	217.0	C2	−1.0	−9.8(5.2)	—
C11	29.8	29.0	30.5	C11	222.5	224.5	219.4	C3	−7.8	10.3	7.9
C12	21.7	22.8	29.9	C12	231.8	235.7	208.7	C4	14.4	2.4	2.6
C16	12.7	13.1	12.0	C16	224.3	232.5	232.3	C5	19.8	19.6	11.0
C17	1.0(0.4)		12.8	C17	214.5		237.5	C6	−3.6	0.1	9.6
C18	14.4			C18	238.9			C7	—	−5.6	−7.4
C19	**1.2(−5.0)**	10.2(9.1)		C19	209.9	225.9		C8	−12.6(6.5)	−1.5	3.7
C20	8.7	16.4		C20	190.6(77.3)			C9	−6.1	7.0	−0.3
N14		7.9(7.1)		N14		191.7(77.5)		C10	8.3	16.5	9.8
N1			17.4	N1			195.3(76.8)	C11	−4.0	−4.3	−1.4
C21			**0.2(−0.4)**	C21			214.4	C12	0.4	3.4	−11.7(3.0)
C22			11.1	C22			244.1				
C23			15.4	C23			208.9				
C24			14.5	C24			239.0				

Table 3 Gibbs free energy (Δ_rG^0, kcal mol^{-1}) at 298.15 K of the FHT, PL, and RAF reaction of **C1–C3** towards HO$^\bullet$ radical in the gas phase. Corresponding values calculated in water are only given (in parentheses) for the most spontaneous reactions. All calculations are performed at the M05-2X/6-311++G(d,p) level of theory

HAT				PL				RAF			
Pos.	**C1**	**C2**	**C3**	Pos.	**C1**	**C2**	**C3**	Pos.	**C1**	**C2**	**C3**
C9	−4.4	−2.3	−2.6	C9	437.0	432.1	434.3	C2		−39.3(−23.6)	—
C11	−1.9	−2.7	−1.3	C11	439.8	441.7	436.6	C3	−33.0	−16.3	−7.9
C12	−10.0	−8.9	−1.9	C12	449.0	453.0	425.9	C4	−9.8	−21.7	−10.4
C16	−19.1	−18.6	−19.7	C16	441.5	449.7	449.5	C5	−4.2	−3.3	−2.5
C17	−30.7(−33.6)		−18.9	C17	431.8		454.7	C6	−28.1	−23.2	−4.5
C18	−17.3			C18	456.1			C7	−17.8	−32.1	−26.7(−24.6)
C19	−30.5(−38.9)	−21.6(−24.8)		C19	427.1	443.1		C8	−41.6(−21.6)	−27.7	−16.1
C20	−23.0	−15.4		C20	407.9(79.7)			C9	−31.6	−32.2	−15
N14		−23.8(−26.8)		N14		408.9(80.0)		C10	−15.0	−5.7	−2.1
N1			−14.4	N1			412.5(79.2)	C11	−30.7	−30.7	−16.6
C21			−31.6(−34.4)	C21			431.7	C12	−24.0	−20.4	−26.6(−24.2)
C22			−20.6	C22			461.3				
C23			−16.4	C23			426.1				
C24			−17.3	C24			456.3				

Table 4 Gibbs free energy (Δ_rG^0, kcal mol^{-1}) at 298.15 K of SET reaction towards HOO$^\bullet$/HO$^\bullet$ free radical

	HOO$^\bullet$			HO$^\bullet$		
	C1	**C2**	**C3**	**C1**	**C2**	**C3**
Gas	145.1	144.8	145.5	129.7	129.5	130.2
Water	37.4	37.2	41.1	15.3	15.2	19.0

formal hydrogen transfer (FHT), proton loss (PL), radical adduct formation (RAF), and single electron transfer (SET) mechanism ((R4)–(R7)). The Gibbs free energies (Δ_rG^0) of HAT, PL and RAF reactions between antioxidant and HOO$^\bullet$ and HO$^\bullet$ radicals at various positions are shown in Tables 2 and 3, respectively. The reaction *via* SET mechanism, which is considered position-independent, is separately presented in Table 4.

As shown in the Table 2, in the gas phase, the Gibbs free energy values (Δ_rG^0) for FHT reaction (R4) towards HOO$^\bullet$ are positive at all H-donating positions, ranging from 0.2 to 30.5 kcal mol^{-1}. This result indicates that the potential for HOO$^\bullet$ removal *via* FHT mechanism of all three investigated compounds is not spontaneous and not favorable. Concerning the RAF mechanism (R6), the Δ_rG^0 found negative values at some specific positions. For example, the **C1** compound shows highly negative Δ_rG^0 of −13.0 and −12.6 kcal mol^{-1} at C7 and C8 positions, respectively. For **C2**, HOO$^\bullet$ RAF process is highly favorable at C2 position with Δ_rG^0 being −9.8 kcal mol^{-1}. Finally, for **C3**, the RAF reaction favorably occurs at C2 and C12 positions with Δ_rG^0 value being −14.2 and −11.7 kcal mol^{-1}, respectively. Thus, the RAF is the only responsible mechanism for the scavenging process towards HOO$^\bullet$ radical in the gas phase. However, in water, HOO$^\bullet$ scavenging is only favorable with FHT mechanism but not with RAF. Indeed, spontaneous Δ_rG^0 are only obtained *via* FHT mechanism for **C1** (at C19 position, −0.5 kcal mol^{-1}) and **C3** (at C21 position, −0.4 kcal mol^{-1}). Finally, the proton transferring process (PL, (R5)) has positive Δ_rG^0 at all positions; thus, the ability to remove HOO$^\bullet$ free radicals by PL process is neither favored in the gas phase nor in water.

Regarding to the OH$^\bullet$ scavenging activities (Table 3), the negative Δ_rG^0 values are obtained at all positions of three studied compounds for both the FHT and RAF processes. This proves that **C1–C3** have high scavenging potential towards OH$^\bullet$ radical *via* FHT and RAF processes. The most active compound *via* FHT mechanism is awarded for **C1** (C17 position) and **C3** (C21 position), with the Δ_rG^0 of −30.7 and −31.6 kcal mol^{-1}, respectively. The lowest Δ_rG^0 values for RAF mechanism are obtained for **C1** (C8 position) and **C2** (C2 position) compounds with the values in the gas phase of −41.6 and −39.3 kcal mol^{-1}, respectively. For the proton transfer process, positive values of Δ_rG^0 are observed at all the positions for all aaptamines. This result is reasonable because the gas phase is not a favorable medium for the charge transfer process like the proton transfer. In gas phase, the RAF scavenging towards OH$^\bullet$ is more favorable than the FHT. For example, **C1** has the lowest Δ_rG^0(FHT) being −30.7 kcal mol^{-1}, whereas it has the lowest Δ_rG^0(RAF) being −41.6 kcal mol^{-1}. In contrast, in water, the FHT is more competitive than the RAF. For example, the lowest Δ_rG^0(FHT) of **C1** is lowered to −38.9 kcal mol^{-1} at C19, while the lowest Δ_rG^0(RAF) is obtained for **C3** with −24.6 kcal mol^{-1} at C18 position. In contract to this, the PL process is always not spontaneous and not favorable in any medium.

Moreover, the Gibbs free energies of the SET reactions (R7) are not favorable in our conditions with the Δ_rG^0 value in the gas phase varying around 145 kcal mol^{-1} for HOO$^\bullet$ radical and 130 kcal mol^{-1} for HO$^\bullet$ radical (Table 4). Although the Δ_rG^0 have been significantly decreased in water (15–41 kcal mol^{-1}), the electron transfer is obviously not spontaneous.

Table 5 Gibbs free energy of activation ($\Delta G^{\ddagger}$, in kcal mol^{-1}) at standard concentration (1 M) and TST rate constant (k_{TST}, in cm^3 per molecule per s) including the Eckart tunneling correction at 298.15 K calculated in the gas phase for FHT, RAF and SET reactions of **C1–C3** towards HOO$^{\bullet}$ radical. Calculations are performed at the M05-2X/6-311++G(d,p) level of theory

Reaction	$\Delta G^{\ddagger, 1\ M}$, kcal mol^{-1}	$k_{TST}^{298.15\ K}$, cm^3 per molecule per s
FHT		
C1@C19H + HOO$^{\bullet}$	16.8	9.10×10^{-19}
C2@N14H + HOO$^{\bullet}$	19.3	2.60×10^{-21}
C3@C21H + HOO$^{\bullet}$	19.8	2.30×10^{-19}
Ascorbic + HOO$^{\bullet}$	9.2	3.10×10^{-15}
RAF		
C1@C8 + HOO$^{\bullet}$	14.8	3.40×10^{-19}
C2@C2 + HOO$^{\bullet}$	14.0	3.80×10^{-18}
C3@C12 + HOO$^{\bullet}$	15.6	7.60×10^{-21}
Ascorbic + HOO$^{\bullet}$	15.0	3.60×10^{-19}
SET		
C1 + HOO$^{\bullet}$	420.9	4.30×10^{-295}
C2 + HOO$^{\bullet}$	378.7	3.93×10^{-264}
C3 + HOO$^{\bullet}$	401.3	1.05×10^{-280}

Overall, the radical scavenging activities of the studied compounds favorably occur *via* RAF mechanism in the gas phase while in water it more likely occurs *via* HAT mechanism. The HO$^{\bullet}$ radical scavenging is much more favorable than the reaction with HOO$^{\bullet}$. Finally, the antioxidant potential *via* HAT process of the three studied compounds is classified in the increasing trend: **C2** < **C3** ≈ **C1**. For RAF mechanism, **C1** and **C2** are potent in gas phase while the **C3** is more active in water.

3.4. Kinetics

In order to identify the main existing form of **C1–C3** (*i.e.* neutral, protonated or deprotonated forms) at the physiological condition (pH = 7.4), pK_a value needs to be determined.[56] The pK_a of three aaptamines **C1–C3** were calculated at the M05-2X/6-311++G(d,p) level of theory. Similar calculation for aniline at the same level of theory was performed for comparison; the obtained value of pK_a is 31.1 at 298.15 K for aniline, consistent with the experimental data, *i.e.* 30.6 or 28.0, reported in DMSO and in water, respectively.[57,58] For our aaptamines, the result shows that pK_a of **C1–C3** are of 22.8, 23.6 and 22.4, respectively. Therefore, the neutral form of **C1–C3** in water is considered in the following calculations.

The kinetics of the possible reactions was studied with the neutral forms of **C1–C3** in gas phase and water, for the OOH$^{\bullet}$ scavenging. The Gibbs free energy of activation ($\Delta G^{\ddagger}$) and transition state theory (TST) rate constant (k_{TST}) for all reactions were systematically calculated at the M05-2X/6-311++G(d,p) level of theory. Gibbs free energy of activation and TST rate constants obtained in the gas phase are presented in Table 5. Optimized structures of the transition states (TSs) for FHT and RAF reaction in both phases are presented in the Fig. 3 and 4. Cartesian coordinates and thermochemical properties for TSs of HAT and RAF reactions between three aaptamines derivatives with HOO radical are resumed in Tables S2 and S3, ESI file.†

For FHT reaction, the compounds **C1** and **C3** display the activation Gibbs free energy of 16.8 and 19.8 kcal mol^{-1}, respectively. Similar rate constants are obtained for two compounds **C1** and **C3** (~10^{-19} cm^3 per molecule per s), which is much smaller than the one of a standard antioxidant such as ascorbic acid calculated in the same condition (~10^{-15} cm^3 per molecule per s). For the RAF reaction, the lowest activation Gibbs free energy $\Delta G^{\ddagger}$ (14.0 kcal mol^{-1}) and the highest rate constant (3.80×10^{-18} cm^3 per molecule per s) are obtained for **C2** at C2 position, indicate the most favorable reaction. At the second place, the **C1** is found with similar activation Gibbs free energy as ascorbic acid, values of about 14.8–15.0 kcal mol^{-1} and rate constants of 3.4–3.6 × 10^{-19} cm^3 per molecule per s. In the contrary, the SET reaction is found with very high activation energy of about 400 kcal mol^{-1} and near-zero rate constants.

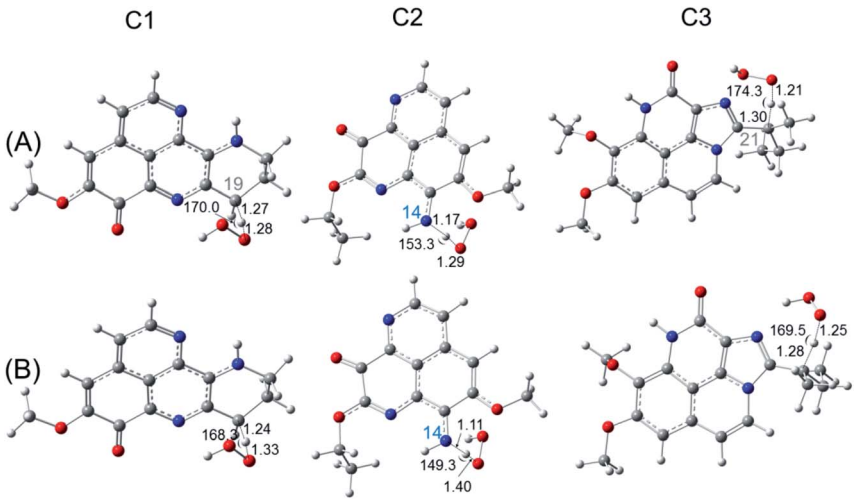

Fig. 3 Optimized structures of the transition state for FHT reaction of **C1**, **C2**, **C3** with HOO$^{\bullet}$ radical in the gas phase (A) and in water (B) at the easiest H donating positions. Calculations are performed at the M05-2X/6-311++G(d,p) level of theory.

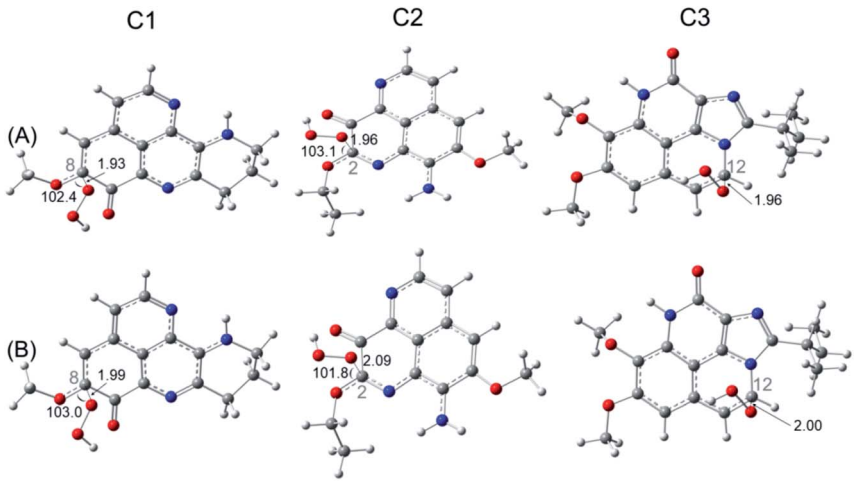

Fig. 4 Optimized structures of the transition state for RAF reaction of **C1**, **C2**, **C3** with HOO˙ radical in the gas phase (A) and in water (B) at the most spontaneous addition positions. Calculations are performed at the M05-2X/6-311++G(d,p) level of theory.

For the reactions in water, kinetics data including the Gibbs free energy of activation $\Delta G^{\ddagger}$, the diffusion rate constants k_D, thermal rate constant k_T, Eckart-tunneling-corrected rate constants k_{eck}, diffusion-corrected rate constants k_{app}, and the branching ratio Γ (%) for each reaction FHT, RAF and SET are resumed in Table 6.

For FHT reaction at the C19H position of **C1**, it happens to be a barrierless reaction, with negative Gibbs free energy of activation (-0.87 kcal mol^{-1}). Moreover, the rate constant obtained at this position is of 7.13×10^6 M^{-1} s^{-1}. On the contrary, the FHT reaction of **C3** requires 5.17 kcal mol^{-1} of Gibbs free energy of activation and appears with a rate constant of only 3.84×10^3 M^{-1} s^{-1}. Moreover, FHT reaction is not favored for the **C2** with very high reaction barrier (22.2 kcal mol^{-1}) and even lower apparent rate constant (6.10 M^{-1} s^{-1}). For RAF reaction, the reaction barriers ($\Delta G^{\ddagger}$) are found to be 5.6, 7.2 and 7.5 kcal mol^{-1} for **C1**, **C2**, **C3**, respectively. As can be seen in the Table 6, the diffusion rate constants k_D of RAF are of about 10^9 M^{-1} s^{-1}, while the thermal rate constants are much smaller ($\sim 10^5$ M^{-1} s^{-1}). The RAF apparent rate is observed with **C2** at the C2 position with $k_{app} = 1.40 \times 10^5$ M^{-1} s^{-1} while a double k_{app} values ($2.8–2.9 \times 10^5$ M^{-1} s^{-1}) are obtained for **C1** and **C3.** These results show higher reaction rate of **C2** and **C3** *via* RAF than *via* FHT mechanism. Similar as in the gas phase, the SET reaction of all three compounds requires very high activation Gibbs free energy (45–53 kcal mol^{-1}) and occurred at extremely small rate (10^{-25} to 10^{-20} M^{-1} s^{-1}). Overall, we observed a competition of the FHT and RAF reaction for the HOO˙ scavenging depending on the chemical nature of the substituents to the aaptamine. For **C1**, the FHT reaction is dominant with branching ratio being 96%, while the HOO˙ scavenging *via* RAF is more favored with **C2** and **C3** with Γ values being 100% and 99%, respectively.

3.5. Formal H transfer – HAT or PCET?

In order to answer the question how and whether or not the electron and proton are transferred in many important energy conversion processes in chemistry and biology,[59] the chemical nature of the FHT process for the aaptamine derivatives with HOO˙ radical is analyzed in this section. Identifying the HAT

Table 6 Gibbs free energy of activation ($\Delta G^{\ddagger}$, kcal mol^{-1}), diffusion rate constant (k_D, M^{-1} s^{-1}), TST thermal rate constant (k_T, M^{-1} s^{-1}), Eckart-tunneling-corrected rate constants (k_{eck}, M^{-1} s^{-1}), diffusion-corrected apparent rate constants (k_{app}, M^{-1} s^{-1}) and branching ratio Γ (%) calculated at 298 K for the FHT, RAF and SET mechanism with HOO˙ radical in water

Reaction path	$\Delta G^{\ddagger}$, $^{1\,M}$, kcal mol^{-1}	k_D, M^{-1} s^{-1}	k_T, M^{-1} s^{-1}	k_{eck}, M^{-1} s^{-1}	k_{app}, M^{-1} s^{-1}	Γ, %
FHT						
C1@C19H + HOO˙	−0.87	1.40×10^9	7.17×10^6	3.22×10^{-15}	7.13×10^6	96
C2@N14H + HOO˙	22.2	2.60×10^9	3.60×10^{-4}	6.10×10^0	6.10×10^0	0
C3@C21H + HOO˙	5.17	1.27×10^9	3.84×10^3	3.22×10^{-16}	3.84×10^3	1
RAF						
C1@C8 + HOO˙	7.2	2.10×10^9	3.00×10^7	2.80×10^5	2.80×10^5	4
C2@C2 + HOO˙	5.6	2.20×10^9	4.20×10^8	1.40×10^5	1.40×10^5	100
C3@C12 + HOO˙	7.5	2.00×10^9	1.90×10^7	2.90×10^5	2.90×10^5	99
SET						
C1 + HOO˙	47.10	8.22×10^9	4.56×10^{-21}	—	4.56×10^{-21}	0
C2 + HOO˙	45.91	8.26×10^9	3.35×10^{-20}	—	3.35×10^{-20}	0
C3 + HOO˙	53.19	8.47×10^9	1.55×10^{-25}	—	1.55×10^{-25}	0

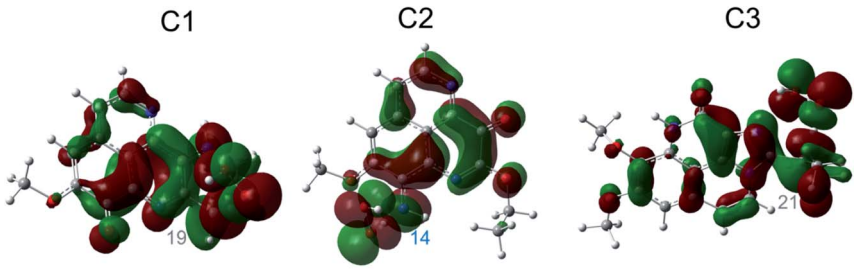

Fig. 5 SOMO distributions of the transition states (TSs) for FHT reactions at the easiest H donating positions.

and PCET mechanisms is a difficult mission because the same reactants and the same products are recognized between these two mechanisms, although the reaction pathways are totally different. Analyses of singly occupied molecular orbital (SOMO) distribution (Fig. 5) and of electronic properties such as NPA charges, atomic spin densities (ASD), natural electron configuration (NEC) calculated at the transition states (TSs) (Table S4, ESI file†) as well as NBO analyses (Table S5, ESI file†) allow addressing this problem.

Fig. 5 represents first the SOMO distributions at the TSs for FHT reactions of three aaptamine compounds with HOO˙ radical in the gas phase. It is reported that SOMO of HAT TSs is distributed with significant densities in orbitals along the H-shifting vector between the donor and acceptor, while the one of PCET TSs is orthogonal to the transition vector.[60] As can be seen in Fig. 5, the 2p orbitals of the acceptor (*i.e.* O34 and O44 atom of the HOO˙ radical) and the one of the donor (*i.e.* C atoms or N14 atom) are interacted and distributed along the H-shifting vector whereas the π-electrons on the HOO˙ radical and the ones on the aromatic rings of aaptamines are tunneled together. This observation consists in the first signal for a H atom transfer (HAT) nature.

To shed more light into changes of electron densities at the transition states of FHT processes, we investigated natural bond orbitals (NBO) analysis (Table S5, ESI file†). As a result, for the FHT reaction between **C1** and HOO˙ at the C19H position (**C1**@C19H + HOO˙), the electron densities are transferred from the first σ-bonding of C19–H bond, σ(1) C19–H, to the first σ-antibonding of O34–O35 bond, σ*(1) O34–O35, with a stabilization energy [*E*(2)] of 7.7 kcal mol^{-1}. Conversely, the electron densities are also transferred from the lone pairs of electron on O34 atom of HOO˙ radical, LP(1) O34, LP(2) O34 and LP(3) O34, to the σ*(1) C19–H with the E(2) values being 324.3, 27.2 and 255.8 kcal mol^{-1}, respectively. For the reaction **C2**@N14H + HOO˙, only the electron transfer from σ-antibonding of N14–H bond, σ*(1) N14–H, to the one of O34–O35 bond, σ*(1) O34–O35, is observed with a small *E*(2) value of 5.5 kcal mol^{-1}. A similar observation is found the reaction **C3**@C21H + HOO˙. In fact, the electron densities are essentially changed from σ*(1) C21–H to σ*(1) O34–O35 with the stabilization energy *E*(2) being 1293.7 kcal mol^{-1}. In the reverse trend, the electrons from the lone pair on O44 and O45 atoms, LP(1) O44 and LP(1) O45, of the HOO˙ radical to the first σ-antibonding on C21–C24 bond, σ*(1) C21–C24, with the *E*(2) values being 5.6 and 77.5 kcal mol^{-1}, respectively.

Furthermore, natural electron configuration (NEC) of the TSs in Table S5† of ESI shows that the mitigated-H species have 1s occupancy $1s^{0.61-0.67}$ which likely corresponds to one H atom with configuration $1s^{1.0}$. In addition, the ASD values of the H species at the transition state are slightly varying from −0.05014 to −0.01012. This result is in good agreement with the one observed for HAT reaction of α-mangostin with HOO˙ radical.[60] Moreover, the NEC of carbon centered-donors in **C1** and **C3** shows the configurations $2s^{0.96-1.02}2p^{3.20-3.31}$ likely $2s2p^3$, while the one of nitrogen-based donor in **C2** has the configuration $2s^{1.39}2p^{4.25}$ likely $2s2p^4$. In the same time, the H-acceptors (*i.e.* O34 and O44 atoms) have the electron configurations $2s^{1.80-1.82}2p^{4.49-4.56}$ which are similar with the $2s^22p^4$. In addition, the spin densities are all distributed at the donors (0.26019–0.46482) and at the acceptors (0.32787–0.42642). These observations support the conclusion that the shifted-H has an atom character rather than a proton one. Thus, the FHT processes of all three aaptamines have the chemical nature of HAT mechanism.

3.6. Indirect antioxidant potential *via* copper ions chelating properties

Besides ferric ion [*i.e.* Fe(III)], the cupric ion Cu(II) consists in one of the most abundant cations available in most organisms and in human body.[18] Although they are themselves not harmful species, their reduction can lead to the formation of very reactive hydroxyl HO˙ radical *via* the Haber–Weiss cycle.[61] Regarding to Cu(II) ion, its complexation with the potential antioxidant compounds could sometime prevent the reduction process that forms Cu(I) ion and HO˙ radical. The fact was that, several potential antioxidants show good copper ions chelating abilities were reported with aminoguanidine,[62] pyridoxamine,[63] lipoic and dihydrolipoic acids,[64] purine,[18] citric acid,[65] D-penicillamine,[66] 2-hydroxymelatonin and 4-hydroxymelatonin.[16] In this study, the Cu(II) complexes formed by the chelating process of the three aaptamines at different possible chelation sites in water phase are evaluated; the results are presented in Fig. 6. Similar complexes with Cu(I) ion are also presented in Fig. 7. Standard enthalpies (ΔH^0) and Gibbs free energies (ΔG^0) of the complexation processes ((R8) and (R9)) are determined to evaluate the stability of the obtained complexes. Only bidentate complexes with the hydrated copper ions, *i.e.*

$[Cu(I)\cdot 4H_2O]^+$ and $[Cu(II)\cdot 4H_2O]^{2+}$ are considered because they are more stable than the monodentate ones as showed by several studies in the literature. Cartesian coordinates and thermochemical properties for the complexes between three aaptamines derivatives with Cu(II) and Cu(I) ions are presented in the Tables S6 and S7, ESI.†

As can be seen in Fig. 6, all three aaptamine compounds show spontaneous and favorable Cu(II) ion chelating activities with negative ΔH^0 and ΔG^0 values. Indeed, the most favorable chelating site for **C1** is found at O14/N1 with $\Delta H^0/\Delta G^0$ being $-4.3/-10.4$ kcal mol^{-1}. Similarly, the most favorable site for **C2** is at O17/N1 with $\Delta H^0/\Delta G^0$ being $-4.8/-10.8$ kcal mol^{-1}, and for **C3** being at O18/N19 ($\Delta H^0/\Delta G^0$ being $4.5/-2.2$ kcal mol^{-1}). Thus, the Cu(II) ion chelating activities of three studied compounds can be ranged in the increasing trend: **C3** < **C1** < **C2**. The Cu(II) chelation of the studied aaptamines are better than the one of aminoguanidine (ΔG^0, 13.8 kcal mol^{-1}),[62] 2-hydroxymelatonin and 4-hydroxymelatonin (ΔG^0, -5.59 and 0.63 kcal mol^{-1}, respectively)[16] and D-penicillamine (ΔG^0, 0.3 kcal mol^{-1}).[66]

Furthermore, it is noteworthy that the Cu(I) complexation is more favorable than the one of Cu(II) ion for all three compounds at the same chelation site. For example, the ΔH^0 and ΔG^0 values of the complexation process at the O14/N1 site of **C1** are -9.4 and -15.4 kcal mol^{-1}, respectively. For **C2** at the O17/N13 site, the formed Cu(I) complex is also stable with $\Delta H^0/\Delta G^0$ being $-7.5/-13.7$ kcal mol^{-1}, while the $\Delta H^0/\Delta G^0$ values for **C3** at the O18/N19 chelating site are equal to $-9.9/-15.7$ kcal mol^{-1}. It is noted that the Cu(I) chelating activities

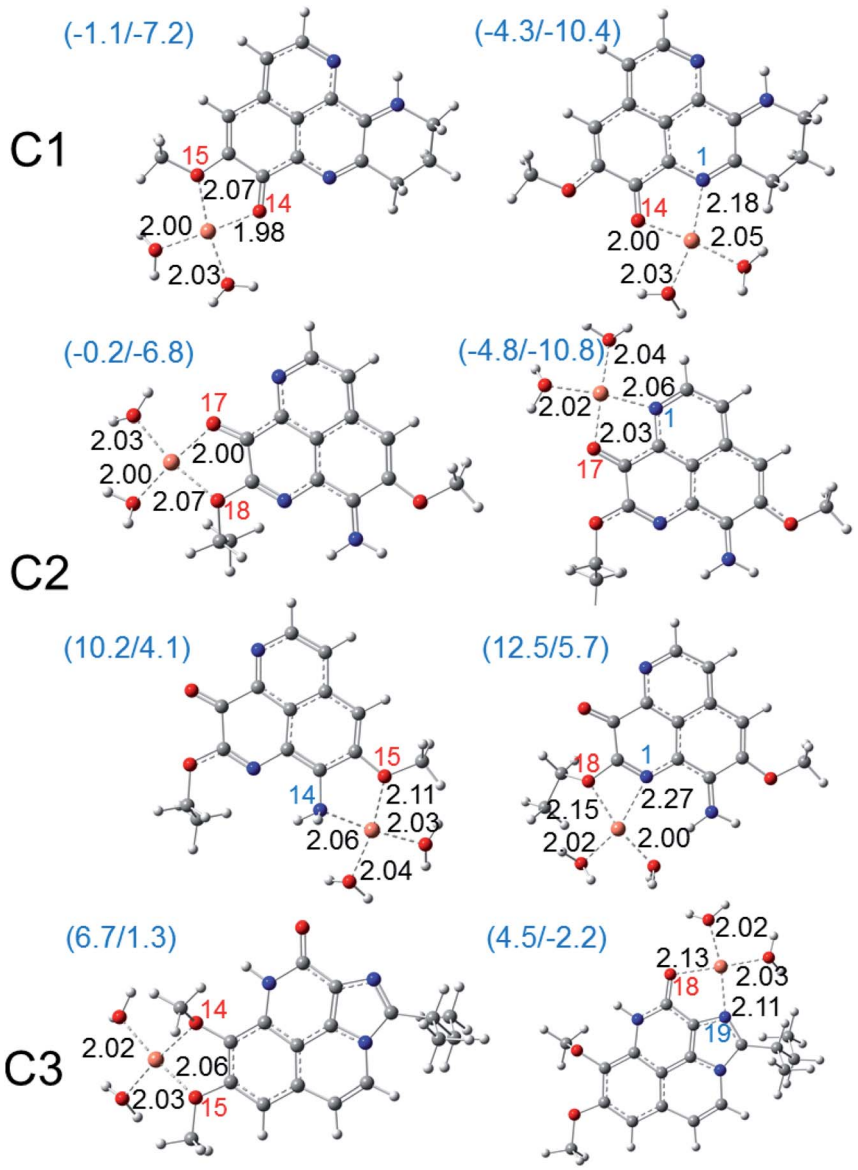

Fig. 6 Optimized structures of the bidentate Cu(II) complexes of three aaptamines **C1**–**C3** in water phase calculated at the M05-2X functional with the basis set LanL2DZ for Cu and the 6-311++G(d,p) for other elements. The standard enthalpies (ΔH^0) and Gibbs free energies (ΔG^0) of the complexation reactions in kcal mol^{-1} are given in the parentheses. Coordinated oxygen and nitrogen atoms are numbered in red and blue, respectively. Bond distances (in angstroms) are noted in black.

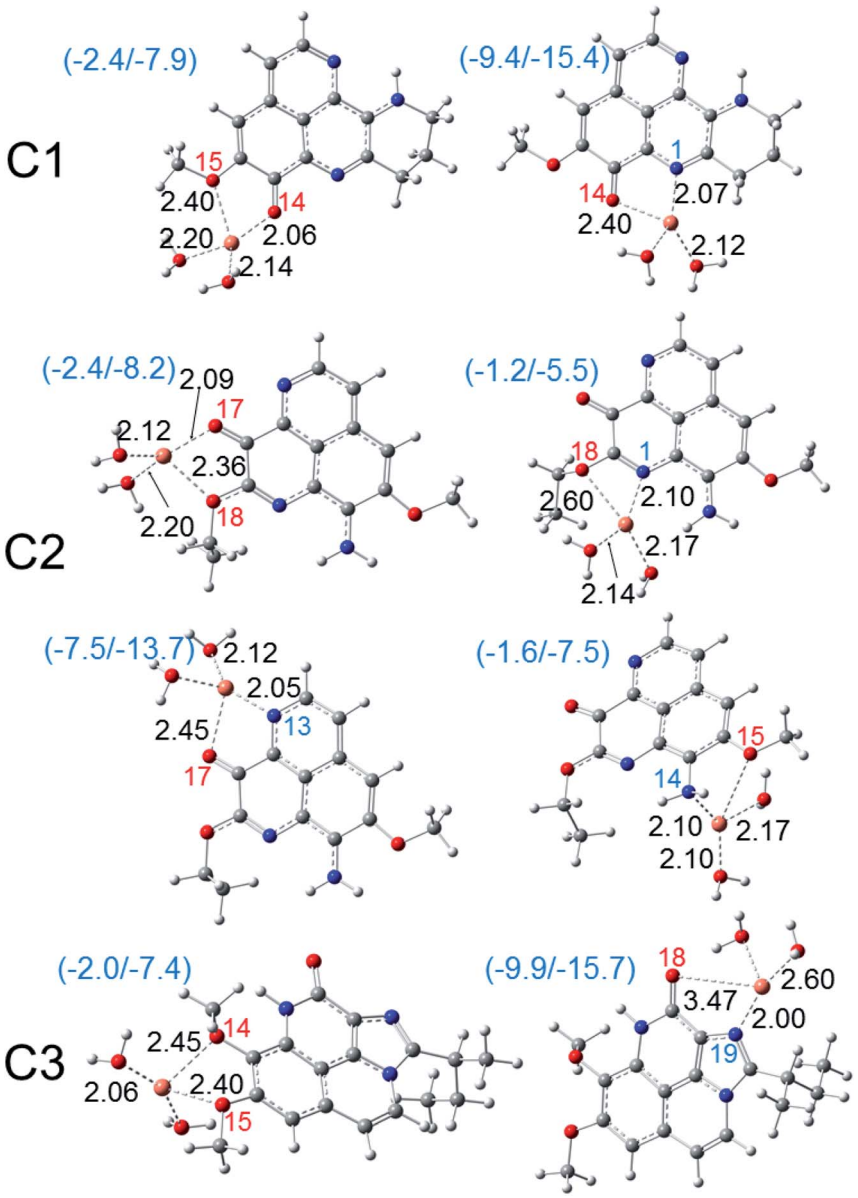

Fig. 7 Optimized structures of the bidentate copper(I) complexes of three aaptamines **C1–C3** in water phase calculated at the M05-2X functional with the basis set LanL2DZ for Cu and the 6-311++G(d,p) for other elements. The standard enthalpies (ΔH^0) and Gibbs free energies (ΔG^0) of the complexation reactions in kcal mol^{-1} are given in the parentheses. Coordinated oxygen and nitrogen atoms are numbered in red and blue, respectively. Bond distances (in angstroms) are noted in black.

are in the increasing order: **C2** < **C1** < **C3**, which is in the reverse order in comparison with the Cu(II) ones.

Thus, all three aaptamine derivatives present the spontaneous and favorable formation of the complexes with both Cu(II) and Cu(I) hydrated ions in water phase. This reduces the availability of these ions to participate in the Haber–Weiss cycle in forming the hydroxyl radical.

3.7. UV radiation absorption properties

The vertical excitation of the molecules **C1–C3** is studied with TD-DFT using different functionals such as B3LYP, B98, M06, PBE0, CAM-B3LYP and M05-2X as previously recommended for accuracy.[52] In order to compare with experimental data reported in MeOH,[4] all calculation is performed in MeOH using the implicit model IEF-PCM. The lowest absorption wavelength of each compound calculated by six above-mentioned functionals is presented in the Table S8† of ESI in comparison with the measured data.

As can be seen in Table S8,† among the different methods, a fairly consistent result in comparison with the experimental data is obtained with CAM-B3LYP and M05-2X functional. For example, the lowest absorption of **C1** calculated in MeOH by M05-2X is found at 423 nm while the experimental value was reported at 398 nm in the same solvent (25 nm deviation). Similar deviation of about 30 nm was obtained for **C2**. However,

Table 7 Vertical excited energies (eV), absorption wavelength (nm), oscillator strength *f* and the corresponding electronic transition of some lowest excited states of **C1–C3** calculated by TD-DFT at the M05-2X/6-311++G(d,p) level in MeOH

Cp	ES	*E*/eV	*A*/nm	*f*	Transition	%
C1	S_1	2.93	423	0.3553	H → L	96
	S_3	3.60	345	0.1614	H−1 → L	91
	S_7	4.84	257	0.4625	H−2 → L	47
					H → L+1	43
	S_8	5.33	233	0.1603	H → L+2	92
		5.72	212	0.0277	H−1 → L+1	62
					H → L+3	24
C2	S_1	2.87	435	0.2938	H → L	97
	S_3	3.78	328	0.1196	H−1 → L	86
					H−3 → L	6
	S_6	5.01	248	0.6778	H → L+1	77
					H−1 → L	8
					H−3 → L	8
	S_8	5.24	237	0.1734	H → L+2	83
					H−3 → L	8
C3	S_1	4.24	292	0.1447	H → L	86
					H−1 → L+1	8
	S_3	4.90	253	0.5688	H → L+1	45
					H → L+2	21
					H−1 → L	15
					H−1 → L+2	9
	S_4	5.22	238	0.1517	H−1 → L+2	72
					H−1 → L	13
					H → L+2	6
					H → L+1	5
	S_5	5.46	227	0.9586	H → L+2	55
					H−1 → L	15
					H−1 → L+1	8
					H−1 → L+2	8
					H → L+1	7
	S_7	5.71	217	0.2460	H-1 → L+2	49
					H-2 → L	18
					H → L+2	15
					H → L+6	5

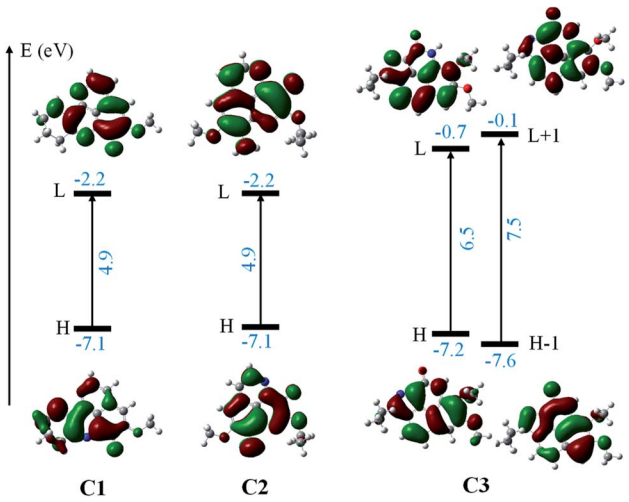

Fig. 8 The energy gap and energy levels of the frontier molecular orbitals which participated to the lowest electronic transition of **C1–C3**. The result is obtained at the TD-DFT/M05-2X/6-311++G(d,p) level in MeOH (IEF-PCM).

a much higher deviation is observed with **C3**, for which a shorter wavelength of 292 nm is absorbed *vs.* 350 nm in measurement. The other methods, which comprise a portion of 20–30% HF in exchange correlation, give much less-comparative absorption. For example, the B3LYP functional (20% HF) provides much higher absorption wavelengths, *i.e.* 471, 482 and 332 nm for **C1–C3**, respectively. As discussed in the literature, the main drawback of TD-DFT consists of the underestimation of the vertical excited energy, for which a significant error up to 0.4 eV can be found.[67] However, for comparative purpose, the TD-DFT results in general can still provide a benefit when it treats with the same kind of molecules.

The vertical excited energy of some lowest excitations calculated by TD/M05-2X/6-311++G(d,p) as well as the oscillator strength and the nature of the corresponding electronic transition are presented in Table 7. Vertical excitations of **C1**, **C2**, and **C3** are found at 2.93, 2.87 and 4.24 eV, respectively. In all cases, we observed mainly the contribution of the HOMO to LUMO transition for the lowest lying excitation of **C1–C3**. This contribution varies from 96% for **C1**, 97% for **C2** and 86% for **C3**. As predicted in the electronic properties part, the HOMO and LUMO of three compounds involved mostly the rings of aaptamine derivatives, then all the lowest absorption is mainly characterized as π–π* transition.

Finally, the Fig. 8 displays the energy gap and energy level of the frontier molecular orbitals that participated to the lowest electronic transition of the **C1–C3**. One can easily notice that: (i) there is a much lower gap (4.9 eV) for **C1** and **C2** in comparison with 6.5 eV gap in case of **C3**, and (ii) possessing the same energy level for HOMO, the energy level of LUMO of **C1** and **C2** is much lower than that of **C3**. All results indicate that the **C1** and **C2** can be more easily excited than **C3**. This agrees with the TD-DFT results, that the **C1** and **C2** absorbed the deep blue and UVA radiation (423/345 and 435/328 nm) while the **C3** is effective UVB (292 nm) absorption agent. The results suggest the use of aaptamines **C1–C3** as photo-protective agents.

4. Conclusions

The antioxidant activities of three aaptamines (**C1**, **C2** and **C3**) extracted from sponges was investigated in the gas phase and water using DFT method according to four mechanisms: HAT, SET, PL and RAF. First, all of these investigated compounds exhibited the best antioxidant activity *via* RAF mechanism, for which antioxidant potential is classified in the increasing order **C2** < **C1** < **C3** for $HOO^{\bullet}$ and **C3** < **C2** < **C1** for $HO^{\bullet}$ free radical scavenging activity. Furthermore, HAT mechanism is elucidated as the second competitive mechanism, in particularly for $HO^{\bullet}$ quenching and in water. Thermodynamically, the antioxidant activities *via* four studied processes are in the decreasing order as follows: RAF > HAT > SET > PL (gas) and HAT > RAF > SET > PL (water). Kinetic calculation shows that the HAT mechanism is the most favorable path for $HOO^{\bullet}$ scavenging in water with **C1**

while the RAF is more competitive with **C2** and **C3**. Second, all three aaptamine derivatives exhibit spontaneous and favorable complexation with both the Cu(I) and Cu(II) hydrated ions in water. The Cu(II) ion chelating activity is classified in the increasing order: **C3** < **C1** < **C2**, whereas the Cu(I) complexation is in the reverse order: **C2** < **C1** < **C3**. Third, all compounds are effective in the UVA and UVB absorption. Within the range of our study, the M05-2X level provides the best performance for calculation of vertical excited energy using TD-DFT. These results promote aaptamine derivatives as natural antioxidant and anti-UV agents for the use in human healthcare such as in pharmaceutics and cosmetics.

Conflicts of interest

The authors declare no conflict of interest.

Acknowledgements

This research is funded by Vietnam National Foundation for Science and Technology Development (NAFOSTED) under grant number 103.01-2019.380. The authors are grateful for the help in kinetic calculation from Dr Thi Chinh Ngo (Duy Tan University). The authors are also grateful to the Gridchem (http://www.seagrid.org) for providing computer resources using the Extreme Science and Engineering Discovery Environment (XSEDE) supported by the USA National Science Foundation grant number ACI-10535. Dorra Khiri, Sonia Taamalli, Florent Louis, and Abderrahman El Bakali appreciated the support from the LABEX CaPPA (Chemical and Physical Properties of the Atmosphere), which is funded by the French National Research Agency (ANR) through the PIA (Programme d'Investissement d'Avenir) under contract ANR-11-LABX-0005-01 and also the Regional Council "Hauts de France" and the "European Funds for Regional Economic Development".

References

1 K. Shaari, K. C. Ling, Z. Mat Rashid, T. P. Jean, F. Abas, S. M. Raof, Z. Zainal, N. H. Lajis, H. Mohamad and A. M. Ali, *Mar. Drugs*, 2009, **7**, 1–8.
2 L. K. Shubina, A. I. Kalinovsky, S. N. Fedorov, O. S. Radchenko, V. A. Denisenko, P. S. Dmitrenok, S. A. Dyshlovoy, V. B. Krasokhin and V. A. Stonik, *Nat. Prod. Commun.*, 2009, **4**, 1085–1088.
3 C.-D. Pham, R. Hartmann, W. E. G. Müller, N. de Voogd, D. Lai and P. Proksch, *J. Nat. Prod.*, 2013, **76**, 103–106.
4 H. Nakamura, J. Kobayashi, Y. Ohizumi and Y. Hirata, *Tetrahedron Lett.*, 1982, **23**, 5555–5558.
5 H.-B. Yu, F. Yang, F. Sun, J. Li, W.-H. Jiao, J.-H. Gan, W.-Z. Hu and H.-W. Lin, *Mar. Drugs*, 2014, **12**(12), 6003–6013.
6 L. K. Shubina, A. I. Kalinovsky, S. N. Fedorov, O. S. Radchenko, V. A. Denisenko, P. S. Dmitrenok, S. A. Dyshlovoy, V. B. Krasokhin and V. A. Stonik, *Nat. Prod. Commun.*, 2009, **4**(8), 1085–1088.
7 J. J. Bowling, H. K. Pennaka, K. Ivey, S. Wahyuono, M. Kelly, R. F. Schinazi, F. A. Valeriote, D. E. Graves and M. T. Hamann, *Chem. Biol. Drug Des.*, 2008, **71**, 205–215.
8 G. Rajivgandhi, S. N. kumar, G. Ramachandran and N. Manoharan, *Biocatal. Agric. Biotechnol.*, 2019, **17**, 628–637.
9 H.-B. Yu, F. Yang, F. Sun, G.-Y. Ma, J.-H. Gan, W.-Z. Hu, B.-N. Han, W.-H. Jiao and H.-W. Lin, *J. Nat. Prod.*, 2014, **77**, 2124–2129.
10 S. A. Dyshlovoy, S. N. Fedorov, L. K. Shubina, A. S. Kuzmich, C. Bokemeyer, G. Keller-Von Amsberg and F. Honecker, *BioMed Res. Int.*, 2014, **2014**, 469309.
11 S. A. Dyshlovoy, S. Venz, L. K. Shubina, S. N. Fedorov, R. Walther, C. Jacobsen, V. A. Stonik, C. Bokemeyer, S. Balabanov and F. Honecker, *J. Proteomics*, 2014, **96**, 223–239.
12 T. Hamada, Y. Matsumoto, C.-S. Phan, T. Kamada, S. Onitsuka, H. Okamura, T. Iwagawa, N. Arima, F. Tani and C. S. Vairappan, *Nat. Prod. Commun.*, 2019, **14**, 1–3.
13 C.-D. Pham, R. Hartmann, W. E. G. Müller, N. de Voogd, D. Lai and P. Proksch, *J. Nat. Prod.*, 2013, **76**, 103–106.
14 S. Takamatsu, T. W. Hodges, I. Rajbhandari, W. H. Gerwick, M. T. Hamann and D. G. Nagle, *J. Nat. Prod.*, 2003, **66**, 605–608.
15 P. De Luna, E. A. C. Bushnell and J. W. Gauld, *J. Phys. Chem. A*, 2013, **117**, 4057–4065.
16 A. Pérez-González, A. Galano, J. R. Alvarez-Idaboy, D. X. Tan and R. J. Reiter, *Biochim. Biophys. Acta, Gen. Subj.*, 2017, **1861**, 2206–2217.
17 R. Castañeda-Arriaga, J. R. Alvarez-Idaboy and N. Mora-Diez, *RSC Adv.*, 2016, **6**, 107924–107932.
18 R. Castañeda-Arriaga, A. Pérez-González, J. R. Alvarez-Idaboy and A. Galano, *Int. J. Quantum Chem.*, 2018, **118**, e25527.
19 T. H. D. Thao, V. T. N. Dung and D. Q. Dao, *Vietnam J. Chem.*, 2019, **57**, 696–701.
20 G. Mazzone, *J. Phys. Chem. A*, 2019, **123**, 9560–9566.
21 A. Galano, G. Mazzone, R. Alvarez-Diduk, T. Marino, J. R. Alvarez-Idaboy and N. Russo, *Annu. Rev. Food Sci. Technol.*, 2016, **7**, 335–352.
22 D. H. Truong, N. T. A. Nhung and D. Q. Dao, *Comput. Theor. Chem.*, 2020, **1185**, 112905.
23 J. Krutmann, A. Bouloc, G. Sore, B. A. Bernard and T. Passeron, *J. Dermatol. Sci.*, 2017, **85**, 152–161.
24 J. Cadet, T. Douki, J.-L. Ravanat and P. Di Mascio, *Photochem. Photobiol. Sci.*, 2009, **8**, 903–911.
25 A. Fourtanier, D. Moyal and S. Seite, *Photochem. Photobiol. Sci.*, 2012, **11**, 81–89.
26 S. Dunaway, R. Odin, L. Zhou, L. Ji, Y. Zhang and A. L. Kadekaro, *Front. Pharmacol.*, 2018, **9**, 392.
27 M. S. Latha, J. Martis, V. Shobha, R. Sham Shinde, S. Bangera, B. Krishnankutty, S. Bellary, S. Varughese, P. Rao and B. R. Naveen Kumar, *J Clin Aesthet Dermatol.*, 2013, **6**, 16–26.
28 R. Stevanato, M. Bertelle and S. Fabris, *Regul. Toxicol. Pharmacol.*, 2014, **69**, 71–77.
29 J. V Freitas, F. S. G. Praça, M. V. L. B. Bentley and L. R. Gaspar, *Int. J. Pharm.*, 2015, **484**, 131–137.

30 D. D. Peres, F. D. Sarruf, C. A. de Oliveira, M. V. R. Velasco and A. R. Baby, *J. Photochem. Photobiol., B*, 2018, **185**, 46–49.
31 S. Scalia and M. Mezzena, *Photochem. Photobiol.*, 2010, **86**, 273–278.
32 H. Masaki, *J. Dermatol. Sci.*, 2010, **58**, 85–90.
33 B. Rioux, C. Peyrot, M. M. Mention, F. Brunissen and F. Allais, *Antioxidants*, 2020, **9**, 331–345.
34 D. Q. Dao, T. T. T. Phan, T. L. A. Nguyen, P. T. H. Trinh, T. T. Van Tran, J. S. Lee, H. J. Shin and B.-K. Choi, *J. Chem. Inf. Model.*, 2020, **60**, 1329–1351.
35 M. J. Frisch, G. W. Trucks, H. B. Schlegel, G. E. Scuseria, M. A. Robb, J. R. Cheeseman, G. Scalmani, V. Barone, G. A. Petersson, H. Nakatsuji, X. Li, M. Caricato, A. V. Marenich, J. Bloino, B. G. Janesko, R. Gomperts, B. Mennucci, H. P. Hratchian, J. V. Ortiz, A. F. Izmaylov, J. L. Sonnenberg, D. Williams-Young, F. Ding, F. Lipparini, F. Egidi, J. Goings, B. Peng, A. Petrone, T. Henderson, D. Ranasinghe, V. G. Zakrzewski, J. Gao, N. Rega, G. Zheng, W. Liang, M. Hada, M. Ehara, K. Toyota, R. Fukuda, J. Hasegawa, M. Ishida, T. Nakajima, Y. Honda, O. Kitao, H. Nakai, T. Vreven, K. Throssell, J. A. Montgomery Jr, J. E. Peralta, F. Ogliaro, M. J. Bearpark, J. J. Heyd, E. N. Brothers, K. N. Kudin, V. N. Staroverov, T. A. Keith, R. Kobayashi, J. Normand, K. Raghavachari, A. P. Rendell, J. C. Burant, S. S. Iyengar, J. Tomasi, M. Cossi, J. M. Millam, M. Klene, C. Adamo, R. Cammi, J. W. Ochterski, R. L. Martin, K. Morokuma, O. Farkas, J. B. Foresman and D. J. Fox, *Gaussian 16 software*, 2016.
36 Y. Zhao, N. E. Schultz and D. G. Truhlar, *J. Chem. Theory Comput.*, 2006, **2**, 364–382.
37 A. Galano and J. R. Alvarez-Idaboy, *J. Comput. Chem.*, 2013, **34**, 2430–2445.
38 A. Galano and J. R. Alvarez-Idaboy, *J. Comput. Chem.*, 2014, **35**, 2019–2026.
39 J. E. Bartmess, *J. Phys. Chem.*, 1994, **98**, 6420–6424.
40 Z. Markovic, J. Tošovic, D. Milenkovic and S. Markovic, *Comput. Theor. Chem.*, 2016, **1077**, 11–17.
41 E. Dzib, J. L. Cabellos, F. Ortíz-Chi, S. Pan, A. Galano and G. Merino, *Int. J. Quantum Chem.*, 2019, **119**, e25686.
42 Y. Okuno, *Chem. - Eur. J.*, 1997, **3**, 212–218.
43 S. W. Benson, *The foundations of chemical kinetics*, Krieger Pub Co., Malabar, Florida, 1982.
44 R. A. Marcus, *Annu. Rev. Phys. Chem.*, 1964, **15**, 155.
45 F. C. Collins and G. E. Kimball, *J. Colloid Sci.*, 1949, **4**, 425–437.
46 M. V. Smoluchowski, *Z. Phys. Chem.*, 1918, **92**, 129.
47 D. G. Truhlar, *J. Chem. Educ.*, 1985, **62**, 104.
48 A. Einstein, *Ann. Phys.*, 1905, **322**, 549–560.
49 G. G. Stokes, *Mathematical and Physical Papers*, Cambridge University Press, 1905.
50 Y. H. Jang, L. C. Sowers, T. Çağin and W. A. Goddard, *J. Phys. Chem. A*, 2001, **105**, 274–280.
51 G. C. Shields, *Computational Approaches for the Prediction of pKa Values*, CRC Press, 2013.
52 D. Jacquemin, B. Mennucci and C. Adamo, *Phys. Chem. Chem. Phys.*, 2011, **13**, 16987–16998.
53 J. Tomasi, B. Mennucci and E. Cancès, *J. Mol. Struct.*, 1999, **464**, 211–226.
54 D. Farmanzadeh and M. Najafi, *J. Serb. Chem. Soc.*, 2016, **81**, 277–290.
55 T. C. Ngo, T. H. Nguyen and D. Q. Dao, *J. Chem. Inf. Model.*, 2019, **59**, 766–776.
56 L. Muñoz-Rugeles, A. Galano and J. R. Alvarez-Idaboy, *Phys. Chem. Chem. Phys.*, 2017, **19**, 15296–15309.
57 F. G. Bordwell, D. Algrim and N. R. Vanier, *J. Org. Chem.*, 1977, **42**, 1817–1819.
58 F. G. Bordwell and D. J. Algrim, *J. Am. Chem. Soc.*, 1988, **110**, 2964–2968.
59 D. R. Weinberg, C. J. Gagliardi, J. F. Hull, C. F. Murphy, C. A. Kent, B. C. Westlake, A. Paul, D. H. Ess, D. G. McCafferty and T. J. Meyer, *Chem. Rev.*, 2012, **112**, 4016–4093.
60 A. Martínez, A. Galano and R. Vargas, *J. Phys. Chem. B*, 2011, **115**, 12591–12598.
61 F. Haber and J. Weiss, *Naturwissenschaften*, 1932, **20**, 948–950.
62 G. García-Díez, R. Ramis and N. Mora-Diez, *ACS Omega*, 2020, **5**, 14502–14512.
63 J. Ortega-Castro, M. Adrover, J. Frau, J. Donoso and F. Muñoz, *Chem. Phys. Lett.*, 2009, **475**, 277–284.
64 R. Monreal-Corona, J. Biddlecombe, A. Ippolito and N. Mora-Diez, *Antioxidants*, 2020, **9**, 674.
65 A. Martínez, R. Vargas and A. Galano, *Comput. Theor. Chem.*, 2018, **1133**, 47–50.
66 A. Martínez, R. Vargas and A. Galano, *Int. J. Quantum Chem.*, 2018, **118**, e25457.
67 A. Dreuw and M. Head-Gordon, *J. Am. Chem. Soc.*, 2004, **126**, 4007–4016.